Epitaxial Electrodeposition of $Ag(Ag_3O_4)_2NO_3$ onto Highly Oriented Conducting Metal Oxides in the Pb-Tl-O System

Bryan E. Breyfogle, Richard J. Phillips, and Jay A. Switzer*

Department of Chemistry and Graduate Center for Materials Research, University of Missouri—Rolla, Rolla, Missouri 65401

Received June 29, 1992. Revised Manuscript Received August 27, 1992

The conducting oxy salt $Ag(Ag_3O_4)_2NO_3$ has been electrodeposited onto highly oriented conducting oxides of Tl_2O_3 and $Pb_aTl_bO_c$. Tl_2O_3 was grown in a [100] texture while the mixed oxide $Pb_aTl_bO_c$ was grown with two different thickness-dependent textures of [110] and [210]. The orientation of the $Ag(Ag_3O_4)_2NO_3$ crystals with respect to the substrate surface was determined by X-ray diffraction. The face-centered-cubic $Ag(Ag_3O_4)_2NO_3$ crystals deposited on body-centered-cubic Tl_2O_3 and face-centered-cubic $Pb_aTl_bO_c$ followed the orientation of these prelayers. However, $Ag(Ag_3O_4)_2NO_3$ electrodeposited onto polycrystalline 430 stainless steel had a nearly random orientation. The lattice mismatch is 6.6% between Tl_2O_3 and $Ag(Ag_3O_4)_2NO_3$, and it is 7.8% between $Ag(Ag_3O_4)_2NO_3$ and the doubled unit cell edge length of $Pb_aTl_bO_c$. It was also found that $Pb_aTl_bO_c$ undergoes a transition from a body-centered-cubic to a face-centered-cubic Bravais lattice at a lead content (determined on a metals-only basis) of greater than 40 atom %.

Introduction

The occurrence of the silver oxy salt $Ag(Ag_3O_4)_2NO_3$ has been known for quite some time.[1-8] It is one of a series of compounds $Ag(Ag_3O_4)_2X$ where $X = NO_3^-$, ClO_4^-, F^-,[6] HF_2^-, and BF_4^-.[9] The material can be electrodeposited from $AgNO_3$ solutions by the following anode half-reaction:

$$7Ag^+ + NO_3^- + 8H_2O = Ag(Ag_3O_4)_2NO_3 + 16H^+ + 10e^-$$

$Ag(Ag_3O_4)_2NO_3$ has a face-centered-cubic (fcc) Bravais lattice with four formula units per unit cell. It belongs to the cubic space group $Fm3m$ with $a = 0.989$ nm.[10,11] $Ag(Ag_3O_4)_2NO_3$ is believed to contain silver in the +1, +2, and +3 oxidation states.[6,9,11] The crystals have been described as fcc cells consisting of Ag_6O_8 polyhedral cages with Ag(I) located interstitially between the polyhedra and NO_3^- ions at the centers of the polyhedral cages.[12] The Ag(I) is coordinated to eight oxygens at the apexes of a cube.[10] The Ag_6O_8 polyhedral cages formally contain the Ag(II) and Ag(III) coordinated to four oxygen atoms in indistinguishable square-planar ligand fields.[9] $Ag(Ag_3O_4)_2NO_3$ has a small temperature-independent paramagnetism much like that of a metal.[9] It has been shown to display metallic conductivity and is superconducting at 1.04 K.[12] $Ag(Ag_3O_4)_2NO_3$ decomposes in air to AgO, $AgNO_3$, and O_2, over a period of several weeks. This decomposition process is accelerated in boiling water.[6]

Epitaxy has been defined as the growth of crystals on a crystalline substrate that determines their orientation.[13] Our interest in the epitaxial influence of Tl_2O_3 and the mixed oxide $Pb_aTl_bO_c$ stems from previous work involving electrodeposited superlattices based on the $Pb_aTl_bO_c/Pb_dTl_eO_f$ system[14] and the electrochemical and photoelectrochemical deposition of highly oriented Tl_2O_3.[15-17] A minimum requirement for successful superlattice growth is to maintain epitaxy between layers. For epitaxy to occur it is generally assumed that there should be little or no lattice mismatch. In the case of nonmetallic structures with a complex basis (i.e., more than one atom per lattice point) lattice mismatch cannot be discussed simply in terms of the difference in lattice parameters. Bonding constraints must be considered. The overlap of metal–oxygen wave functions should be maximized and the overlap of metal–metal and oxygen–oxygen wave functions should be minimized. We would like to determine whether oxides with apparently quite different crystal structures (e.g., body-centered-cubic (bcc) on fcc) will grow epitaxially. The Pb–Tl–O system was chosen for this study because the electrodeposited films are highly conducting and textured. Also, the crystal structures and textures can be tuned by varying the deposition current density and the film thickness.

A previous nucleation and growth study by Michailova and Milchev of $Ag(Ag_3O_4)_2NO_3$ electrodeposited on the ⟨100⟩, ⟨110⟩, and ⟨111⟩ faces of an fcc platinum single crystal ($a = 0.395$ nm) showed the platinum surface to have no strong epitaxial influence on the $Ag(Ag_3O_4)_2NO_3$ crystals.[18] In this study we investigated the influence of textured prelayer oxides on the orientation of the electrodeposited $Ag(Ag_3O_4)_2NO_3$ crystals. The orientation of the $Ag(Ag_3O_4)_2NO_3$ crystals with respect to the substrate surface was determined by X-ray diffraction and observed by scanning electron microscopy (SEM). The prelayer oxides used were [100]-textured Tl_2O_3, [110]-textured $Pb_aTl_bO_c$, and [210]-textured $Pb_aTl_bO_c$. The materials in this study demonstrate a unique strength of electrodeposition as an atomic level architecture technique, since the

* To whom correspondence should be addressed.

(1) Sulc, O. *Z. Anorg. Chem.* **1896**, *12*, 89.
(2) Sulc, O. *Z. Anorg. Chem.* **1900**, *24*, 305.
(3) Brown, M. *J. Phys. Chem.* **1916**, *20*, 680.
(4) Jirsa, F. *Z. Anorg. Allg. Chem.* **1925**, *148*, 130.
(5) Bailar, J. C., Jr. *J. Chem. Educ.* **1944**, *21*, 523.
(6) McMillan, J. A. *Chem. Rev.* **1962**, *62*, 65.
(7) Adzic, G. D.; Drazic, D. M.; Despic, A. R. *J. Electroanal. Chem.* **1988**, *239*, 107.
(8) Adzic, G. D.; Despic, A. R.; Drazic, D. M. *J. Electroanal. Chem.* **1988**, *241*, 353.
(9) Hindermann, D. K.; Robin, M. B.; Kuebler, N. A. *J. Magn. Reson.* **1969**, *1*, 479.
(10) Wong, C. H.; Lu, T. H.; Chen, C. N.; Lee, T. J. *J. Inorg. Nucl. Chem.* **1972**, *34*, 3253.
(11) Naray-Szabo, I.; Argay, G.; Szabo, P. *Acta. Crystallogr.* **1965**, *19*, 180.
(12) Conway, M. M.; Phillips, N. E.; Gebelle, T. H.; Kuebler, N. A.; McWhan, D. B. *Phys. Rev. Lett.* **1970**, *17*, 917.
(13) Bauer, E. G.; Dodson, B. W.; Ehrlich, D. J.; Feldman, L. C.; Flynn, P. C.; Geis, M. W.; Harbison, J. P.; Matyi, R. J.; Peercy, P. S.; Petroff, P. M.; Phillips, J. M.; Stringfellow, G. B.; Zangwill, A. *J. Mater. Res.* **1990**, *5*, 852.
(14) Switzer, J. A.; Shane, M. J.; Phillips, R. J. *Science* **1990**, *247*, 444.
(15) Switzer, J. A. *J. Electrochem. Soc.* **1986**, *133*, 722.
(16) Phillips, R. J.; Shane, M. J.; Switzer, J. A. *J. Mater. Res.* **1989**, *4*, 923.
(17) Switzer, J. A. *Am. Ceram. Soc. Bull.* **1987**, *66*, 1521.
(18) Michailova, E.; Milchev, A. *J. Appl. Electrochem.* **1988**, *18*, 614.

0897-4756/92/2804-1356$03.00/0

Table I. Composition of $Pb_aTl_bO_c$ Films as a Function of Applied Current Density[a]

current density (mA/cm^2)	potential (V vs SCE)	atom % Pb	atom % Tl
0.06	0.06	46	54
0.62	0.12	66	34
1.24	0.14	71	29
6.20	0.27	88	12

[a] Data in table are taken from ref 14. The solution used to electrodeposit $Pb_aTl_bO_c$ fims was 0.100 M $Pb(NO_3)_2$ and 0.005 M $TlNO_3$, in 5 M NaOH. Atom % Pb and Tl in $Pb_aTl_bO_c$ was determined on a metals-only basis.

metal ions in these materials are in oxidation states that are not accessible by thermal processing.

Experimental Section

The Tl_2O_3 and $Pb_aTl_bO_c$ prelayers were electrodeposited onto polycrystalline 430 stainless steel electrodes purchased from Metal Samples Co. The electrodes were mechanically polished with 600-grit SiC paper and then successively with 1.0-, 0.3-, and 0.05-μm alumina. After polishing, the electrodes were ultrasonically cleaned in a Heat Systems Ultrasonics Model W-385 ultrasonic processor. The electrodes were then pressed tightly in a Teflon holder and rotated at 300 rpm using a PINE Model AFMSRX rotating disk electrode. The area of the polished stainless steel electrode was 1.98 cm^2. All solutions were made from reagent grade chemicals dissolved in doubly distilled deionized water from a Barnstead-NANOpure Ultra Pure water system. Electrochemical depositions were performed using an EG&G Princeton Applied Research Model 273A potentiostat/galvanostat in the galvanostatic mode. All depositions were performed at room temperature (21–25 °C). The solutions from which the oxides were deposited were 0.100 M $TlNO_3$ in 5 M NaOH for Tl_2O_3 and 0.100 M $Pb(NO_3)_2$ and 0.005 M $TlNO_3$ in 5 M NaOH for $Pb_aTl_bO_c$. *Warning*: Lead and thallium salts are extremely toxic. For [100]-textured Tl_2O_3 and [110]-textured $Pb_aTl_bO_c$, the films were grown to a thickness of approximately 5 μm. To achieve a [210] texture in $Pb_aTl_bO_c$, the film was grown to a thickness of approximately 20 μm. These prelayers were all deposited at 5.0 mA/cm^2. The film thicknesses were calculated from the total charge passed assuming 100% current efficiency.

After the prelayer oxides were deposited to the desired thickness, they were thoroughly rinsed with deionized water while still in the Teflon holders and then placed in a 2 M $AgNO_3$ solution. $Ag(Ag_3O_4)_2NO_3$ was then electrodeposited onto the prelayer oxides galvanostatically at 10.0 mA/cm^2 for a total of 10.0 coulomb/cm^2. $Ag(Ag_3O_4)_2NO_3$ was electrodeposited onto a polycrystalline 430 stainless steel electrode under the same conditions as it was deposited onto the prelayers. The electrodes were rotated at 300 rpm.

X-ray diffraction patterns of the prelayers and the $Ag(Ag_3O_4)_2NO_3$ were taken from 2θ = 10–90° on a Scintag 2000 diffractometer using Cu Kα radiation (λ = 0.154 178 nm). SEM micrographs of the $Ag(Ag_3O_4)_2NO_3$ deposits were taken on a JEOL JSM-35CF scanning electron microscope. The metals-only composition of the $Pb_aTl_bO_c$ films was determined by energy-dispersive X-ray analysis in the scanning electron microscope.

Results and Discussion

Orientation and Composition of Conducting Oxide Prelayers. The conditions under which the mixed oxide $Pb_aTl_bO_c$ is electrodeposited affect its composition as well as its orientation. A wide range of Pb/Tl ratios can be achieved from a solution of 0.100 M $Pb(NO_3)_2$ and 0.005 M $TlNO_3$ in strong base by simply changing the applied current density. Table I shows the compositional dependence of the $Pb_aTl_bO_c$ films on applied current density. We have shown previously[14] that the lattice parameter varies by less than 0.3% over the composition range of the films listed in this table.

The textures of the Tl_2O_3 and $Pb_aTl_bO_c$ films are also strongly influenced by the deposition conditions. At a current density of 0.05 mA/cm^2 the oxides grow as a nearly random polycrystalline deposit on 430 stainless steel. However, at a higher current density of 5.0 mA/cm^2, the X-ray diffraction pattern of Tl_2O_3 deposited to a thickness of approximately 5 μm onto 430 stainless steel has an intense Bragg reflection at 2θ of approximately 34° as shown in Figure 1a. The X-ray diffraction pattern of $Pb_aTl_bO_c$ deposited under the same conditions has an intense Bragg peak at 2θ of approximately 48.3° as shown in Figure 1b. These peaks were indexed as the (400) reflection for Tl_2O_3 and the (220) reflection for $Pb_aTl_bO_c$. For $Pb_aTl_bO_c$, the texture of the film also depends on the thickness. If the $Pb_aTl_bO_c$ film is grown to a thickness of approximately 20 μm, the only Bragg peak distinguishable in the X-ray diffraction pattern is the (420) reflection at 2θ of approximately 80.5° as shown in Figure 1c. The high intensities of these reflections relative to others is a good indication of a strongly preferred orientation with the (100) planes parallel to the substrate surface for Tl_2O_3, and the (110) or (210) planes parallel to the substrate surface for $Pb_aTl_bO_c$ film thicknesses of 5 and 20 μm, respectively.

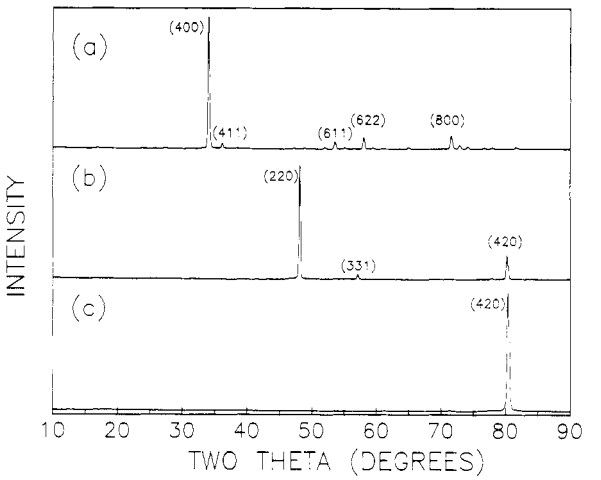

Figure 1. X-ray diffraction patterns of (a) [100]-textured Tl_2O_3, (b) [110]-textured $Pb_{0.8}Tl_{0.2}O_{1.9}$, and (c) [210]-textured $Pb_{0.8}Tl_{0.2}O_{1.9}$.

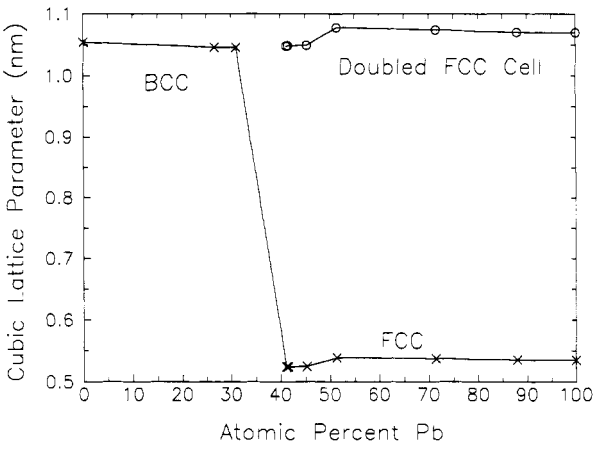

Figure 2. Cubic lattice parameter versus Pb content of electrodeposited $Pb_aTl_bO_c$ films. Notice the bcc/fcc transition for lead contents (determined on a metals-only basis) of greater than 40 atom %. Data for pure fcc PbO_2 is taken from ref 23. (×) measured lattice parameters, (○) lattice parameters assuming doubled fcc unit cell.

Structures of the Conducting Oxide Prelayers. The structure of the $Pb_aTl_bO_c$ is a function of its composition. The $Pb_aTl_bO_c$ system undergoes a transition from a bcc Bravais lattice, like that of Tl_2O_3, to an fcc Bravais lattice at a lead content (determined on a metals-only basis) of

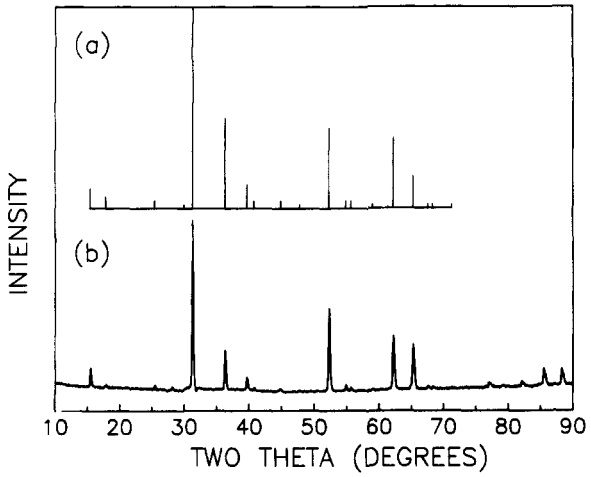

Figure 3. (a) Powder X-ray diffraction pattern of $Ag(Ag_3O_4)_2NO_3$ and (b) X-ray diffraction pattern of $Ag(Ag_3O_4)_2NO_3$ electrodeposited from 2 M $AgNO_3$ at 10.0 mA/cm^2 for 1000 s on 430 stainless steel.

greater than 40 atom % as shown in Figure 2. Assuming all the lead ions are tetravalent and the thallium ions are all trivalent, the formula of the mixed oxide would be given by $Pb_xTl_{1-x}O_{(x+3)/2}$. This is a valid assumption since the overpotentials used to deposit these films are high, thus creating a strong driving force for the oxidation of the metal ions to the +4 and +3 oxidation states. Thus, the composition at the bcc/fcc transition would be $Pb_{0.4}Tl_{0.6}O_{1.7}$. The $Pb_aTl_bO_c$ films used as substrates in this study were electrodeposited at 5.0 mA/cm^2 and have a nominal composition of $Pb_{0.8}Tl_{0.2}O_{1.9}$ and an fcc structure. The actual oxygen content is probably lower, since the highly conducting oxides are nonstoichiometric.

The bixbyite structure of Tl_2O_3 is often described in terms of a distorted fcc fluorite structure with one-quarter of the oxygens missing.[19] In the fluorite structure the coordination number of the oxygens is four, and the coordination number of the metals is eight. In the bixbyite structure the oxygens still have a coordination number of four, but the metal coordination number becomes six. Also, there are two types of metal sites. The missing oxygens for one-quarter of the metals are at the ends of the body diagonal and for the remainder of the metals the missing oxygens are at the ends of the face diagonal. It appears that the substitution of Pb(IV) for Tl(III) in Tl_2O_3 stabilizes an fcc fluorite structure by the addition of oxygen. As Pb(IV) is substituted into thallium(III) oxide, the $MO_{1.5}$ formula of bcc bixbyite approaches the MO_2 formula of fcc fluorite.

The X-ray diffraction patterns of the $Pb_{0.8}Tl_{0.2}O_{1.9}$ films are very similar to the Tl_2O_3 pattern. An important difference between the patterns is that mixed-index reflections such as (411) and (611) are not observed for the $Pb_{0.8}Tl_{0.2}O_{1.9}$ but they are present for Tl_2O_3. This systematic absence of mixed-index reflections is consistent with an fcc structure and is in agreement with the assignment of Sakai et al. for electrodeposited $Pb_{0.6}Tl_{0.4}O_{1.8}$ as an fcc fluorite-type structure with a cubic lattice parameter of 0.533 31 nm.[20] For comparison, Tl_2O_3 has a bcc bixbyite structure with a = 1.054 nm[21] and PbO_2 deposited from alkaline solution is orthorhombic with a = 0.4938 nm, b = 0.5939 nm, and c = 0.5486 nm.[22] Syono and Akimoto have reported an fcc fluorite polymorph of PbO_2 with a = 0.5349 nm produced at high pressure.[23] Table II summarizes the structures for the oxide materials studied in the present paper.

Table II. Structural Summary of the Various Oxides

material	Bravais lattice	a_0 (nm)	space group	ref
$Ag(Ag_3O_4)_2NO_3$	fcc	0.989	*Fm3m*	10, 11
$Pb_{0.8}Tl_{0.2}O_{1.9}$	fcc	0.533	*Fm3m*	14, 20
Tl_2O_3	bcc	1.054	*Ia3*	21

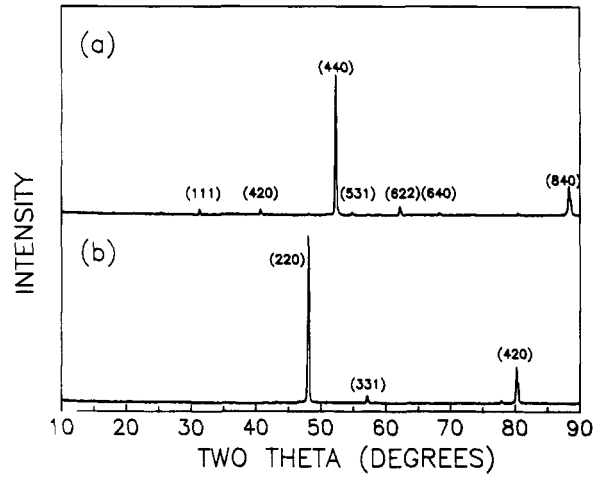

Figure 4. X-ray diffraction patterns of (a) $Ag(Ag_3O_4)_2NO_3$ electrodeposited from 2 M $AgNO_3$ at 10.0 mA/cm^2 for 1000s on a [110]-textured $Pb_{0.8}Tl_{0.2}O_{1.9}$ prelayer and (b) the [110]-textured $Pb_{0.8}Tl_{0.2}O_{1.9}$ prelayer electrodeposited from 0.100 M $Pb(NO_3)_2$, 0.005 M $TlNO_3$ in 5 M NaOH at 5.0 mA/cm^2 to a thickness of 5 μm.

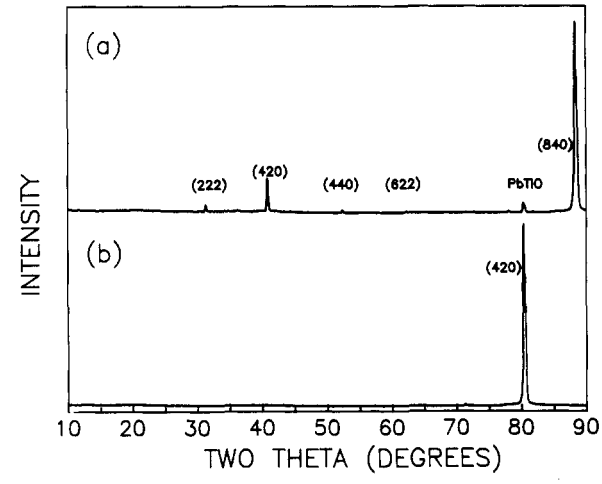

Figure 5. X-ray diffraction patterns of (a) $Ag(Ag_3O_4)_2NO_3$ electrodeposited from 2 M $AgNO_3$ at 10.0 mA/cm^2 for 1000s on a [210]-textured $Pb_{0.8}Tl_{0.2}O_{1.9}$ prelayer and (b) the [210]-textured $Pb_{0.8}Tl_{0.2}O_{1.9}$ prelayer electrodeposited from 0.100 M $Pb(NO_3)_2$, 0.005 M $TlNO_3$ in 5 M NaOH at 5.0 mA/cm^2 to a thickness of 20 μm.

X-ray Diffraction and Scanning Electron Microscopy of Epitaxial $Ag(Ag_3O_4)_2NO_3$ Deposits. The X-ray diffraction pattern for $Ag(Ag_3O_4)_2NO_3$ electrodeposited onto polycrystalline 430 stainless steel is compared to the powder X-ray diffraction pattern for $Ag(Ag_3O_4)_2NO_3$ in Figure 3. This comparison is made to show that without the influence of the textured prelayer oxides $Ag(Ag_3$-

(19) Wells, A. F. *Structural Inorganic Chemistry*, 5th ed.; Oxford University Press: New York, 1991; p 545.
(20) Sakai, M.; Sekine, T.; Yamazaki, Y. *J. Electrochem. Soc.* **1983**, *130*, 1631.
(21) Powder Diffraction File, JCPDS, International Centre for Diffraction Data, Swarthmore, PA; pattern no. 33-1404.
(22) Powder Diffraction File, JCPDS, International Centre for Diffraction Data, Swarthmore, PA; pattern no. 11-549.
(23) Syono, Y.; Akimoto, S. *Mater. Res. Bull.* **1968**, *3*, 153.

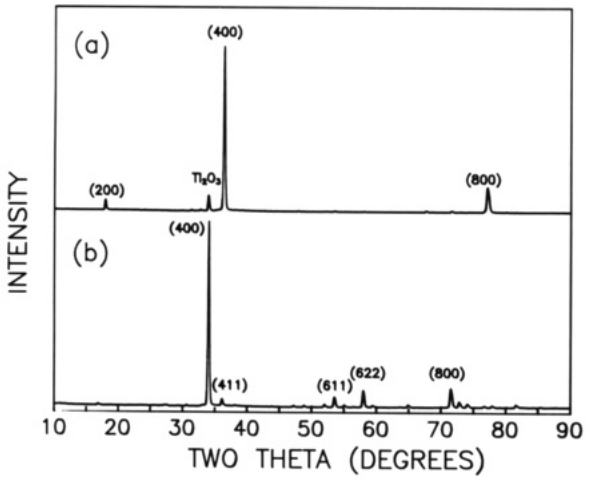

Figure 6. X-ray diffraction patterns of (a) $Ag(Ag_3O_4)_2NO_3$ electrodeposited from 2 M $AgNO_3$ at 10.0 mA/cm^2 for 1000s on a [100]-textured Tl_2O_3 prelayer and (b) the [100]-textured Tl_2O_3 prelayer electrodeposited from 0.100 M $TlNO_3$ in 5 M NaOH at 5.0 mA/cm^2 to a thickness of 5 μm.

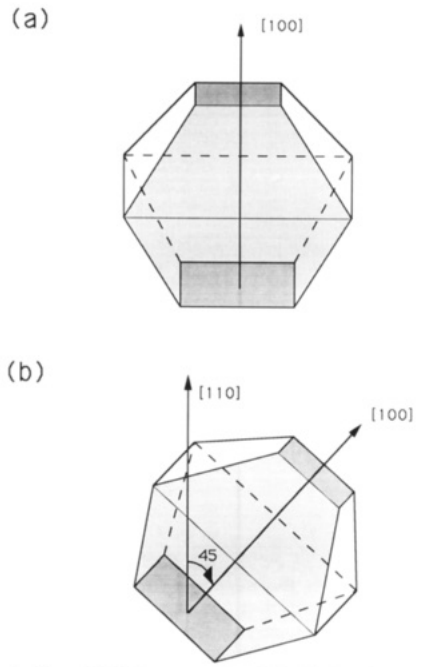

Figure 7. $Ag(Ag_3O_4)_2NO_3$ crystals with (a) [100] orientation and (b) [110] orientation. Notice that in (a) the (100) planes are parallel to the substrate surface and in (b) the (100) planes are tilted 45° with respect to the substrate surface.

$O_4)_2NO_3$ will deposit with a nearly random orientation. Figures 4 and 5 show the X-ray diffraction patterns for fcc $Ag(Ag_3O_4)_2NO_3$ electrodeposited on the two different thickness-dependent textures of fcc $Pb_{0.8}Tl_{0.2}O_{1.9}$. $Ag(Ag_3O_4)_2NO_3$ grows in the same [110] texture as the $Pb_{0.8}Tl_{0.2}O_{1.9}$ in Figure 4, as shown by the intense (440) Bragg reflection at $2\theta = 52.3°$, and it grows in the same [210] texture as the $Pb_{0.8}Tl_{0.2}O_{1.9}$ in Figure 5 as shown by the intense (840) Bragg reflection at $2\theta = 88.6°$. The lattice mismatch between $Ag(Ag_3O_4)_2NO_3$ and the doubled unit cell edge length of $Pb_{0.8}Tl_{0.2}O_{1.9}$ is approximately 7.8%. The X-ray diffraction patterns in Figure 6 are for fcc $Ag(Ag_3O_4)_2NO_3$ electrodeposited onto bcc Tl_2O_3. The mismatch in the cubic lattice parameter between these materials is approximately 6.6%. $Ag(Ag_3O_4)_2NO_3$ follows the orientation of the [100]-textured Tl_2O_3 as seen by the intense (400) reflection for $Ag(Ag_3O_4)_2NO_3$ at $2\theta = 36.3°$. Clearly, we can dramatically influence the orientation of

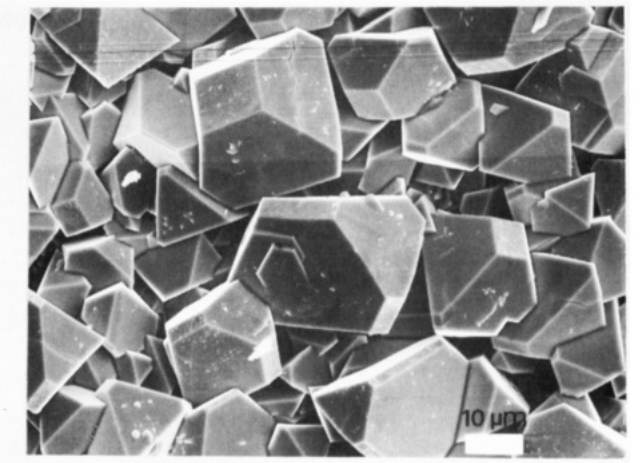

Figure 8. SEM micrograph of [110]-textured $Ag(Ag_3O_4)_2NO_3$ electrodeposited on [110]-textured $Pb_{0.8}Tl_{0.2}O_{1.9}$.

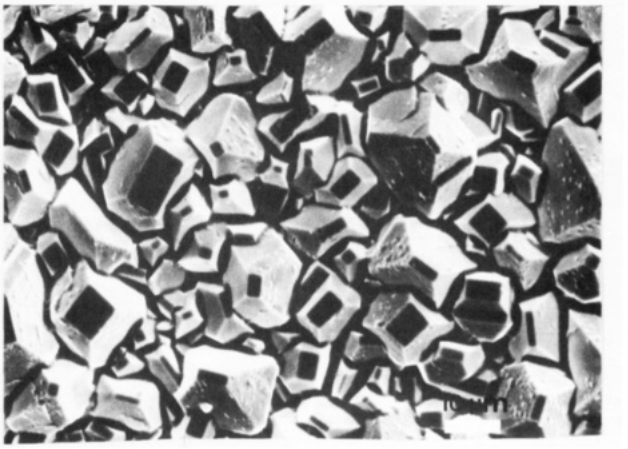

Figure 9. SEM micrograph of [100]-textured $Ag(Ag_3O_4)_2NO_3$ electrodeposited on [100]-textured Tl_2O_3.

the $Ag(Ag_3O_4)_2NO_3$ crystals by electrodeposition onto these textured oxide prelayers.

SEM was employed to visualize the orientation of the $Ag(Ag_3O_4)_2NO_3$ crystals as determined by X-ray diffraction. These crystals are large and regular enough so that their orientation relative to the substrate is distinguishable in the SEM micrographs. An illustration of a $Ag(Ag_3O_4)_2NO_3$ crystal is given in Figure 7 to show the expected microstructure for a [100]-oriented crystal (Figure 7a) and a [110]-oriented crystal (Figure 7b). The X-axis is perpendicular to the substrate. Observe that for a [100]-oriented crystal the (100) planes are parallel to the substrate surface and the [100] direction is normal to the substrate. For the [110]-oriented crystal, the (100) planes are tilted 45° with respect to the substrate surface, and the [110] direction is normal to the substrate surface. The SEM micrograph in Figure 8 is a top view (viewed along the [110] axis) of [110]-textured $Ag(Ag_3O_4)_2NO_3$. Although the angle between the (100) planes and the substrate cannot be measured directly from the micrograph, the (100) planes are consistently tilted with respect to the substrate surface as expected for a [110] orientation. The SEM micrograph in Figure 9 is a top view (viewed along the [100] axis) of [100]-textured $Ag(Ag_3O_4)_2NO_3$. In this micrograph the (100) planes are parallel to the substrate surface as illustrated in Figure 7a.

We have demonstrated that $Ag(Ag_3O_4)_2NO_3$ will grow epitaxially onto both Tl_2O_3 and $Pb_{0.8}Tl_{0.2}O_{1.9}$ by showing that the conducting oxysalt follows the orientation of these conducting oxide prelayers. The next step in our work is to electrodeposit superlattices based on these materials.

This will require that the materials grow by a layer-by-layer two-dimensional mechanism to produce structures with coherent interfaces. We are presently exploring the growth mechanism to determine whether the growth is two-dimensional, or if hemispherical nuclei form which follow the orientation of the prelayer. We also plan to use electrocrystallized $Ag(Ag_3O_4)_2NO_3$ single crystals as substrates for electrodeposited superlattices.

Acknowledgment. This work was supported in part by the Division of Materials Research of the National Science Foundation under Grant No. DMR-9020026 and by the Materials Division of the Office of Naval Research under Grant No. N00014-91-J-1499. We also thank Unocal Corp. for donation of electrochemical instrumentation used in this research.

Registry No. $Ag(Ag_3O_4)_2NO_3$, 12258-22-9; $Pb_{0.8}Tl_{0.2}O_{1.9}$, 144224-58-8; $Pb_{0.4}Tl_{0.6}O_{1.7}$, 144224-59-9; Tl_2O_3, 1314-32-5; 430 stainless steel, 11109-52-7.

Clusters of Immiscible Metals. 2. Magnetic Properties of Iron–Lithium Bimetallic Particles

G. N. Glavee,[1] Kathie Easom,[1] K. J. Klabunde,*[,1] C. M. Sorensen,[2] and G. C. Hadjipanayis[3]

Departments of Chemistry and Physics, Kansas State University, Manhattan, Kansas 66506, and Department of Physics and Astronomy, University of Delaware, Newark, Delaware 19716

Received July 7, 1992. Revised Manuscript Received September 9, 1992

Using low-temperature atom clustering processes, metastable Fe–Li nanoscale particles have been prepared. Upon heat treatment further phase segregation occurred, yielding a core-shell structure of α-Fe clusters surrounded by Li metal. Upon oxidation a coating of Li_2O was formed, but α-Fe particles remained and were protected. Upon CO_2 exposure a Li_2CO_3 protective coating was formed. Saturation magnetization σ values ranged from 100 to 200 emu/g and varied slightly with α-Fe crystallite size. However, coercivities were affected more strongly (and showed a maximum at about 7 nm) and ranged from 20 to 1000 Oe. Mössbauer spectra yielded hyperfine fields and isomer shifts for the various samples. Overall, the protective coatings of Li, Li_2O, and Li_2CO_3 had very little effect on α-Fe particle magnetism, and this is in contrast to the effects of coatings of magnetic materials such as Fe_3O_4. On the other hand, crystallite size effects were significant.

Introduction

The controlled generation of nanoscale α-Fe particles encapsulated and protected by a Li_2CO_3/Li_2O coating was discussed in the first of this series on clusters of immisible metals.[4] The synthetic method involves clustering of Fe and Li atoms in low-temperature matrices yielding metastable Fe_xLi_y clusters (solvated metal atom dispersion, SMAD). The advantages of this approach and the utility of materials generated from it have been described elsewhere.[5-8] The unique properties associated with nanoscale particles have been the subject of a number of recent reviews and publications.[9-11] In addition, the properties of magnetic materials, in particular nanoscale iron particles, have been studied extensively in an effort to develop new materials with higher coercivity and saturation magnetization as well as improve recording density.[12,13]

This work examines the soft magnetic properties of nanoscale α-Fe particles encapsulated by Li metal and, after oxidation, of α-Fe particles encapsulated in Li_2CO_3/Li_2O. For comparison, samples of Fe (without Li) were also studied.

Experimental Section

The preparation and thermal and oxidative processing of Fe–Li and Fe (without Li) samples have been described previously.[4] Crystallite sizes were obtained from X-ray powder diffraction data (Scintag 2000 diffractometer with Cu Kα nickel filtered radiation) and particle sizes from transmission electron microscopy and BET surface area (Micrometics, Flowsorb II 2300 utilizing nitrogen adsorption).[4] Ambient- and low-temperature (77 K) Mössbauer spectra were obtained on a Ranger Scientific Inc. MS-1200 using a cryostat designed by Cryo Industries of America, Inc.

Magnetic properties of the fresh and heat processed samples were obtained using a SQUID magnetometer on weighed samples immobilized and protected by encapsulation in paraffin in a quartz cell at temperatures between 10 and 300 K and in fields up to 55 000 Oe. Elemental analyses were obtained from Galbraith Laboratory, Inc. and the analytical laboratory at Kansas State University.

Results and Discussion

(1) Fe–Li (Fresh) Samples. Mössbauer Spectra and Structural Considerations. The fresh Fe–Li sample has been previously described as a "plum-pudding" structure

(1) Kansas State University, Department of Chemistry.
(2) Kansas State University, Department of Physics.
(3) University of Delaware.
(4) Glavee, G. N.; Kernizan, C. F.; Klabunde, K. J.; Sorensen, C. M.; Hadjipanayis, G. C. *Chem. Mater.* **1991**, *3*, 967.
(5) Klabunde, K. J.; Tanaka, Y. *J. Mol. Catal.* **1983**, *21*, 57.
(6) Klabunde, K. J.; Jeong, G. H.; Olsen, A. W. *Selective Hydrocarbon Activation: Principles and Progress*; Davies, J. A., Watson, P. L., Greenberg, A., Liebman, J. F., Eds.; VCH Publishers: New York, 1990; Chapter 13, pp 433.
(7) Kernizan, C. F.; Klabunde, K. J.; Sorensen, C. M.; Hadjipanayis, G. C. *Chem. Mater.* **1990**, *2*, 70.
(8) Klabunde, K. J.; Davis, S. C.; Hattori, H.; Tanaka, Y. *J. Catal.* **1978**, *54*, 254.
(9) Andres, R. P.; Averback, R. S.; Brown, W. L.; Brus, L. E.; Goddard III, W. A.; Kaldor, A.; Louie, S. G.; Moskovits, M.; Riley, S. T.; Siegal, R. W.; Spaepen, F.; Wang, Y. *J. Mater. Res.* **1989**, *4*, 704.
(10) Matijevic, E. Fine Particles: Science and Technology. *MRS Bull.* **1989**, *14*, 19. Matijevic, E. Fine Particles Part II: Formation Mechanisms and Applications. *MRS Bull.* **1990**, 15, 20.
(11) Ozaki, M. *MRS Bull.* **1989**, *14*, 35.
(12) (a) Tasaki, A.; Tomiyana, S.; Iida, S. *J. J. Appl. Phys.* **1965**, *4*, 707. (b) Hayashi, C. *J. Vac. Sci. Technol. A* **1987**, *5*, 1375.
(13) (a) Nakatani, I.; Furubayashi, T.; Takahashi, T.; Hanoaka, H. *J. Magn. Magn. Mater.* **1987**, *65*, 261. (b) Tang, Z. X.; Nafis, S.; Sorensen, C. M.; Hadjipanayis, G. A.; Klabunde, K. J. *J. Magn. Magn. Mater.* **1989**, *80*, 285. (c) Nafis, S.; Hadjipanayis, G. C.; Sorensen, C. M.; Klabunde, K. J. *IEEE Trans. Magn.* **1989**, *25*, 3641.

0897-4756/92/2804-1360$03.00/0